Mesoporous carbon black-aerogel composites with optimized properties for the electro-assisted removal of sodium chloride from brackish water

G. Rasines[a], P. Lavela[b,*], C. Macías[a], M. C. Zafra[b], J. L. Tirado[b], C.O. Ania[c]

[a] Nanoquimia S.L., PCT Rabanales 21, Ed. Aldebarán M.4.7., 14014 Córdoba, Spain.
[b] Laboratorio de Química Inorgánica, Universidad de Córdoba, Marie Curie, Campus de Rabanales, 14071 Córdoba, Spain.
[c] Instituto Nacional del Carbón (INCAR, CSIC), Apartado 73, 33080 Oviedo, Spain.

Abstract

A simple modification of the sol-gel polymerization of resorcinol-formaldehyde mixtures allowed the preparation route of homogeneously dispersed carbon black-activated carbon aerogel composites with high pore volumes and improved electrical conductivity. These materials showed good performance as electrodes for the electro-assisted removal of sodium chloride from saline water using high voltages. Besides the effect of the carbon black additive, we have investigated the influence of resorcinol-water ratio on the textural and electrochemical properties of the resulting materials. Data has shown a slight dependence on the structural order of the aerogels with the R/W ratio, regardless the incorporation of the conductive additive. The effect of the carbon black on the textural features was also negligible, due to the low amount incorporated. Nonetheless, the samples showed higher capacitance values for the removal of ions from solution, due to the enhanced conductivity provided by the carbon black, being the effect more evident for the materials prepared using a low R/W ratio.

Keywords

Carbon Aerogel; Carbon black; Composite; Electrosorption.

*Corresponding author.

Tel/Fax: 34957218637   E-mail: iq1lacap@uco.es (P. Lavela)

1 Introduction

Drinking water supply is becoming a great concern at the turn of the 21st century. The increasing human population is leading to an overexploitation of water resources for domestic, industrial, and agricultural purposes provoking undesirable fresh water shortages [1]. A reliable solution to supply fresh water may reside in the desalination of brackish water, as long as low-cost technologies are used. Capacitive deionization technology (CDI) is an interesting novel and environmentally friendly method for removing dissolved salts from water. This technology offers outstanding advantages as low maintenance cost and energy consumption, facile regeneration without releasing secondary wastes as compared to other conventional technologies, such as reverse osmosis or evaporation [2-5]. The basic concept of CDI resides in the application of a potential to the electrodes of a symmetric cell composed by highly porous materials. Thus, ions are attracted by the electrodes with opposite charge where remain stored in the electrical double-layer region, similarly to the principle explaining the functioning of an electric double-layer capacitor (EDLC). As a consequence, the salinity of the solution eluted during this charge process has decreased. During the subsequent cell discharge, the potential at the electrodes is switched off and a concentrated solution is separately recovered while the electrodes are regenerated. The electrostatic nature of the ion-electrode interactions ensures a high reversibility during the charge/discharge cycles [6-9].

Numerous carbon materials have been researched in order to meet the requirements of large surface area for ion accumulation, porous morphology for ionic transport and electrical conductivity for effective charge holding. Thus, activated carbons [10, 11], carbon fibers and nanotubes [12, 13], carbon aerogels [14], ordered mesoporous carbons [15], hierarchical porous carbon [16, 17] and graphene [18] have

been envisaged as adequate candidates as electrodes for capacitive deionization. Also, large success has been achieved using carbon electrodes modified by adding metal oxides such as TiO_2 [19], SiO_2 [20], Fe_3O_4 [21] or more recently ZnO [22]. Among them, carbon aerogels prepared from the sol-gel polycondensation of resorcinol-formaldehyde have demonstrated to be electrode materials with great potential in many electrochemical applications [23]. The supercritical drying preserves the pore structure existing in the hydrogel precursor, while their physicochemical and structural properties can be conveniently adapted by modifying the parameters of the synthesis, particularly the reactants (i.e., resorcinol, formaldehyde, water) molar ratios [24-29]. Although carbon gels typically exhibit electrical conductivities higher than other types of aerogels (which are generally insulating materials) and most nanoporous carbons (excluding carbon nanotubes, graphenes or graphitic carbons), the conductivity of resorcinol-formaldehyde derived carbon gels is still a drawback that can limit their implementation. Hence, for most electrochemical applications, carbon electrodes are manufactured adding a small amount carbon black as conductive additive to lower the resistance and thus enhancing the performance of the electrodes [30-32]. In a previous study we have reported the synergistic effect of adding the carbon black during the polymerization of resorcinol-formaldehyde mixtures on the electrochemical and porous features of the resulting carbon/carbon composites [33]. Besides the expected increase in the electrical conductivity, the conductive additive had a large impact on the textural development of the aerogels, directing the synthesis towards the formation of less branched polymer clusters leading to materials with large pore volumes within the micro/mesoporous range. Several authors have also reported the beneficial effect of blending carbon black with activated carbons for improving their electrosorption capacity [31, 32].

In this study we have modified the synthesis by reducing the amount of the carbon black additive added before the hydrogel polymerization stage to ensure a high dispersion of the additive in the carbon gel matrix. Besides investigating the textural features of the carbon black/carbon aerogel nanocomposites, the aim of this work was to determine the electrosorption capacity for NaCl removal of the prepared electrodes. For this purpose we have synthesized activated carbon aerogels using three different resorcinol-water ratios allowing the polymerization of the carbon precursors in the presence or absence of the carbon black additive. The structural and morphological properties of the electrode materials have been characterized by several techniques and the capacitive performance has been determined by cyclic voltammetry and deionization experiments.

2 Materials and methods

2.1 Materials preparation

The carbon gels were synthesized by the sol gel polymerization of resorcinol (R) and formaldehyde (F) in water (W), using sodium carbonate (C) as catalyst, carbon black (CB, Superior Graphite Co.) as conductive additive. Three different aerogels were obtained by setting the R/W ratio at 0.04, 0.06 and 0.08, while the R/F molar ratio was set at 0.5, the R/C at 200 and the amount of carbon black added to the solution was ca. 0.9% w/v. In a typical synthesis, the reagents were placed into sealed glass moulds under magnetic stirring and allowed to undergo gelation and aging in an oven at 40 º C for 24 h and 70 ºC for 120 h. After the water-acetone exchange, the samples were dried under CO_2 supercritical conditions. Finally, the aerogels were subjected to activation at 750 ºC for 3 hours under a CO_2 stream (heating ramp of 2 ºC min^{-1}). For the sake of comparison, a second series of carbon gels was prepared by the same synthetic route

without the incorporation of the carbon black (control series). The samples will be labeled as CAGWX or CAGWX/CB where X determines the R/W ratio, and /CB indicates the presence of carbon black in the composite when it applies.

2.2 Structural and textural characterization

X-Ray diffraction (XRD) patterns were recorded with a Bruker D8 Discover A25 diffractometer furnished with Cu Kα radiation and a graphite monochromator. The patterns were scanned between 10 and 80º (2 theta degrees) at a 0.025º/s scan rate. Raman spectroscopy was performed by excitation with green laser light (532 nm) in the range between 1000 and 2000 cm^{-1}. The spectra were acquired in a Renishaw Raman instrument (InVia Raman Microscope), equipped with a Leica microscope. The profiles were deconvoluted by using the Peakfit v. 4.11 software package. X-ray Photoelectron Spectrometry (XPS) was performed in a SPECS Phobios 150MCD spectrometer provided with Al K source and a chamber pressure of 4×10^{-9} mbar. Powdered samples were deposited as thin films on a holder and subjected to high vacuum overnight. The C 1s line of the adventitious carbon located at 284.6 eV was used as reference for binding energy values. The nanotexture of the prepared gels was characterized by measuring nitrogen adsorption-desorption isotherms at -196 ºC (ASAP 2010, Micromeritics). Before the experiments, the samples were outgassed under vacuum (ca. 10^{-3} torr) at 120 ºC overnight. The isotherms were used to calculate the specific surface area, S$_{BET}$, and total pore volume, V$_T$. The pore size distributions were calculated by using the density functional theory (2D-NLDFT) approach; the micropore volume was also evaluated by the DR method.

2.3 Electrochemical characterization

Electrochemical measurements were performed in three-electrode SwagelokTM type cells. The working electrode consisted of 90 wt.% of the carbon aerogel active material (samples CAGWX/CB) and 10 wt.%, binder (polyvinylidene fluoride). In the case of the control series (samples CAGWX), 20 wt.% of carbon black was added to the mixture of active material (70 wt.%) and binder (10 wt.%). The powdered mixtures were then slurred in N-methyl pyrrolidone and the resulting paste was spread on a 13 mm titanium disk current collector. The electrodes were dried at 70ºC overnight. A platinum wire was used as a counter electrode, while the cell potential was measured versus a Hg/Hg_2SO_4 (SME) reference electrode. A 0.1 M solution of NaCl in deionized water was used as electrolyte. Cyclic voltammograms were recorded between -0.5 and +0.5 V vs. SME at sweep rates ranging from 0.5 to 10 mV s^{-1} in a Biologic VMP multichannel potentiostat. Electrochemical impedance spectroscopy (EIS) allowed analyzing the kinetic response of the electrodes to the adsorption reaction. The spectra were recorded in an Autolab PGSTAT12 system, using an AC voltage signal of 5 mV vs. equilibrium potential over the frequency range 25 kHz to 10 mHz.

2.4 Capacitive deionization

Capacitive deionization experiments were performed in symmetric batch-type cells assembled with two monolithic electrodes previously cut and polished to achieve a flat surface. The monoliths were washed in deionized hot water for 30 minutes and then assembled between titanium current collectors using two Whatman glass GF/A fiber sheets as a separator. This symmetric cell was immersed in 15 mL of the electrolyte under continuous stirring to avoid mass transfer restrictions from the bulk solution. The deionization experiments were carried out by applying constant voltage pulses of 0.9, 1.2 or 1.5 V for 120 min, while the electrode discharge underwent at 0 V for the same

6

period of time. A conductivity meter was used to monitor the change in the ionic concentration. Adsorption rate values were calculated from the sloping part of the deionization curves measured at a short time of one hour and referred either to the area of the volume of the monolith. The experiments were performed in duplicates, and a few cycles were recorded for each sample to check reproducibility; results revealing disparity were discarded.

3 Results and discussion

3.1 Characterization of the aerogels

We have synthesized carbon /carbon aerogel composites by a modification of the sol-gel polymerization of R/F precursors reported by Pekala and co-workers [23], consisting on incorporating a conductive additive to the reactants mixture before the polycondensation reaction. As additive we have used a carbon black commonly used in electrochemical applications, characterized by a low ash and volatile matter content and a high electrical conductivity provided by an ordered structure (see TEM images in Fig. 1). In our previous study we investigated effect of the amount of carbon black added on the electrochemical and porous features of the materials [33]. For additions between 5 and 10 wt.% (covering commonly used percolator mass ratio in electrochemical applications), the aerogels displayed an enhanced conductivity and high pore volumes within the micro-mesopore range, although the synthesis presented some difficulties associated to the dispersion of the carbon black in the solution. To overcome this, we have focus on lowering the loading of the additive (down to 0.9 wt.%) to facilitate the dispersion -hence shortening the synthesis time-, while varying the R/W ratio between 0.04 to 0.08.

Based on our previous studies and given the low amount of carbon black incorporated, we did not expect any modification on the structure of the aerogels, as the chemical pathway of the sol-gel reaction (ca. addition reactions between the precursors, cross-linking and growth of clusters) is the same in the presence of the carbon black [33]. The lack of swelling during the solvent exchange stage confirmed the cross-linking of the clusters. However, the appearance of the carbon aerogels changed slightly upon the incorporation of the carbon black; all the materials become opaque and dark regardless the R/W ratio, as opposed to typical translucent light red color of the control aerogels before the thermal treatment (see Fig. S1 in supplementary information). Additionally, as the R/W ratio increased, the monoliths incorporating the carbon black additive appeared twisted and bent. The aerogel monoliths were synthesized in cylindrical shape, and although the diameter of the disk was the same for all three series, the specimens prepared using low amount of water (high R/W) in the presence of the carbon black showed a concave curvature. This finding had not been observed for higher amounts of carbon black and low R/W molar ratio.

Transmission microscopy images confirmed that the incorporation of the carbon black did not modify the gels structure compared to conventional synthesis (Fig. 1). For the sake of comparison, the micrograph of pure carbon black has also been included. As seen, the aerogel samples are characterized by slightly packed aggregates of nanometric carbon particles (Fig. 1) surrounded by the agglomerates of hollow spherical particles with an average diameter of ca. 30 nm corresponding to the carbon black (see arrow in the images).

A more detailed analysis of the structure of the carbon aerogels can inferred from XRD and Raman spectroscopy. The XRD patterns of all the samples show the broad bands at ca. 22.1 and ca. 44.5º(2θ) ascribed to the (002) and (100) reflections

characteristic of a highly distorted carbon structures (Fig. 2). The contribution of carbon black to the composite samples is clearly revealed by a narrow reflection at ca. 25.5º (2θ) ascribable to the 002 reflection of the more crystalline/ordered phase characteristic of carbon blacks. This fact can be easily verified by observing the pattern of the carbon black used during the synthesis which has been also included in figure 2. Additional signals attributable to the carbon black phase could not be clearly discerned. The same trend was observed by Raman spectroscopy; although the profiles of the spectra were quite similar (Figure S2 in supplementary information), the deconvolution of the spectra allowed a precise evaluation of the I_G/I_{D1} ratio as a measurement of the degree of structural ordering (Table 1). On increasing the R/W ratio, a slight decrease in the I_G/I_{D1} values is observed for both series (with and without carbon black). Concerning the effect of carbon black, I_G/I_{D1} values were slightly higher indicating an overall enhancement in the crystallinity of the samples, although a separated contribution of the carbon black to the spectrum could not be clearly observed.

The evolution of the porous features of the prepared aerogels was very dependent on the synthesis conditions. Fig. 3 and Table 2 show the main textural parameters determined by nitrogen adsorption at -196ºC. All the isotherms can be classified as type IV according to BDDT classification, regardless the presence of the carbon additive and for the three studied R/W ratio. The micropore structure is revealed by the large adsorbed volumes at relative pressures below 0.2. Otherwise, the presence of large (meso)pores is evidenced by the prominent hysteresis loops located at relative pressures above 0.7 in all the series.

It is interestingly observed that the incorporation of the carbon black does not seem to have a large effect on the development of the porosity, as opposed to our previous observations [33]. We attribute this difference to the low amount of carbon

black used in this work, compared to the 5-10 wt.% previously reported. On the other hand, the effect of R/W is much more evident, particularly in the mesopore range. All the samples displayed quite close microporosity and surface areas as inferred from the values compiled in Table 2. In contrast, the mesoporosity followed a different trend; first of all, the total pore (and mesopore) volumes increased as the R/W decreases, whereas the position of the hysteresis loop shifted towards higher relative pressures with the R/W ratio, confirming the enlargement of the mesopores as the R/W decreased. Similar effects on the R/W ratio have been reported in the literature [34,35]. Furthermore the hysteresis loops displayed different shapes; for the samples obtained with R/W of 0.04, the loop is very narrow with quite parallel adsorption and desorption branches (type H1), characteristic of pore systems with uniform pore size distributions. As the R/W increases, the loop widens showing a smooth long adsorption branch and steep desorption (type H2). These pore systems are characterized by broad and heterogeneous distributions of interconnected pores. Table 2 summarizes the main textural parameters obtained from the gas adsorption data. Both the surface area and micropore volumes remained rather unchanged with the R/W ratio, regardless the incorporation of the carbon black. In turn, the mesopore volumes gradually decreased with the R/W ratio, with both series (control and CB) showing the same behavior.

Regarding surface functionalization, details on the chemical composition and the different forms of O-groups provided by XPS analysis are listed in Table 3 and Fig. 4. The C1s core level spectrum of samples was deconvoluted to five contributions (Fig. 4A), The intense peak at 284.6 eV is ascribable to graphitic carbon in sp^2 configuration (284.6 eV), C–OH in phenolic, alcoholic or eteric moieties (286.1±0.1 eV), C=O in carbonyl or quinone (287.3±0.1 eV), and carboxyl or ester (289.7±0.1 eV) groups; the highly broadened band appearing at ca. 291.7±0.1 eV is usually related to shake-up

satellite peaks due to π−π* transitions in aromatic rings [36]. On increasing the R/W ratio, a slightly decrease of the relative contribution of the oxygenated groups is detected. Therefore, we cannot discard some influence of the water concentration at the initial stages of the formation of the hydrogel on the contribution of oxygenated groups attached at the surface of the carbonized aerogel. The addition of carbon black clearly revealed an increase of the relative contribution of C-OH and C=O groups making clear the capability of the conductive carbon to modify the surface functionalization of the final composite. The O1s core level spectra were deconvoluted in four different components (Fig. 4B), assigned to C=O in carbonyl groups (530.9±0.1 eV), lactone, phenol, ether and C–OH (532.6±0.2 eV). A third signal is ascribed to carboxylic acid (534.2±0.2 eV) and a fourth one due to the presence of adsorbed water or oxygen and C=O in occluded CO_2 or CO (536.1±0.1 eV) [37-39]. The relative distribution of O-containing groups remains rather unchanged after the incorporation of the carbon black, apart from a small increase in the contribution of C–O in carbonyl configurations (Table 3). As a general rule, the incorporation of the carbon black slightly increased the surface content of oxygen for all R/W ratio, although the effect was most significant for the aerogel prepared at a R/W of 0.4 (Table 4). This is important since it may significantly improve the hydrophilicity of the aerogels, hence boosting their electrochemical behavior.

3.2 Electrochemical performance of the carbon aerogels

Fig. 5 shows the cyclic voltammograms of the studied aerogels recorded at 0.5 mV s^{-1} in a 0.1 M solution of sodium chloride obtained in a 3-electrode cell. The box-shaped profiles obtained for the carbon black containing composites indicate the predominance of a capacitive behavior due to the accumulation of charge at the electric

double layer at the electrode surface. However, the voltammograms recorded for the non-composited aerogels reveal broadened anodic bands close to 0 mV vs. Hg/Hg_2SO_4 likely related to pseudo-faradaic reactions. This effect has been ascribed to side reaction including the electrolyte decomposition [40], and it seems to be very remarkable for electrodes samples exhibiting high surface areas. Interestingly, the electrodes built on the control aerogel series (samples CAGWx) showed a more resistive behavior, despite ca. 10 wt.% of carbon black was also used for the manufacture of the electrodes. This indicates that the incorporation of the carbon black during the sol-gel polymerization enhances the electrochemical response of the electrodes, even if the amount of conductive additive is lower. This effect has to be attributed to a much better dispersion of the carbon black particles within the aerogel carbonaceous domains during the polycondensation, cross-linking and growth of the clusters. This arrangement does not only creates an interconnect network of large mesopores among the nanograins, but enables the connectivity through the carbon black particles. All this facilitates the ion transport from the electrolyte to the small micropores.

Regarding capacitance, higher values were recorded for CAGW4 (92 F g^{-1}) with the lowest R/W ratio, compared to CAGW6 (77 F g^{-1}) and CAGW8 (77 F g^{-1}). These results follow the expected trend based on the surface areas and micropore volumes of the aerogels, revealing the interesting performance of carbon aerogels prepared at a low R/W ratio. The addition of carbon black provoked a significant increase in the capacitance values, according to the sequence: CAGW4/CB (97 F g^{-1}) > CAGW6/CB (87 F g^{-1}) > CAGW8/CB (84 F g^{-1}). However attempts to correlate this result with the textural features of the aerogels failed, due to the small changes in the surface areas and micropore volumes when the carbon black is incorporated to the synthesis, indicating that the porosity is not the only factor to be considered. To understand this behaviour

the enhancement in the structural ordering as seen by Raman spectroscopy (Table 1) and the noticeable increase in the electrical conductivity provided by the carbon black homogeneously dispersed in the carbon aerogel matrix must be taken into account as crucial factors for the improvement of the electrosorption capacity of these composites. Cyclic voltammograms recorded at fast rates are also shown in Fig. 5; in this case the rectangular shape progressively became a leaf-like shape, accompanied by a decrease in the capacitance values. Thus it is clear that even though the carbon black improved the electrochemical features of the aerogels, still the electrodes cannot deliver fast charge propagation rates, likely due to the relatively low amount of carbon black additive present in the samples. Hence the electrochemical behavior at fast charge rates is more dependent on the conductivity of the electrodes than on the porous features that would assure the fast ionic diffusion from the bulk to the inner pores [41].

Impedance spectra recorded on freshly assembled cells allowed the evaluation of the internal electrode resistance to the ion migration at the carbon aerogel through the electrode/electrolyte interface. Fig. 6 depicts the Nyquist plots for the activated aerogels with and without the carbon black additive, with the characteristic profiles composed of a semicircle followed by a straight line. Impedance data were fitted to an equivalent circuit consisting on a constant phase element (CPE) in parallel to a Warburg impedance (W), and the polarization resistance (R_{pol}) as the measurement of the internal resistance to the ion migration through the electrode pore structure, connected in series to the bulk resistance of the solution (R_{el}) [42, 43]. For our system the contribution of the R_{el}, was neglected (high-frequency response) and the R_{pol} was determined from the real impedance of the semicircle located at intermediate frequencies [42, 43]. As a general rule, increasing the R/W ratio resulted in an increase in the R_{pol}, with the lowest R_{pol} values obtained for CAGW4 (0.45 $\Omega \times g$) and CAGW4/CB(0.59 $\Omega \times g$). As for the

incorporation of the carbon black, no clear dependence was observed as the R_{pol} values of both series were rather close, except for the above-mentioned CAGW4 samples prepared with the lowest R/W molar ratio. The values followed the order: CAGW6/CB (0.80 $\Omega \times g$) < CAGW6 (0.84 $\Omega \times g$), and CAGW8/CB (0.92 $\Omega \times g$) < CAGW8 (0.99 $\Omega \times g$). Nevertheless, the results point out to a close relationship between the polarization resistance values and the mesoporosity, that would act as an intermediate path favoring the migration of ions from the electrolyte to the inner micropores. Indeed, we have observed similar trends with the mesoporosity of aerogel electrodes prepared with different R/C ratio and pH conditions [24, 44].

3.3 Capacitive deionization performance of monolithic electrodes

Monoliths of the activated aerogels and their corresponding composites with carbon black were used to prepare electrodes and perform deionization experiments in symmetric cells (2-electrode configuration). The electrosorption curves upon a charge/discharge cycle were measured at various constant voltage pulses and are displayed in Fig. 7. These plots show the higher electrosorption capacity of sample CAGW4 as compared to its counterparts with different R/W ratios. Thus, 9.4 mg/g NaCl were adsorbed in this sample, compared to only 5.6 and 5.3 mg/g NaCl adsorbed for CAGW6 and CAGW8, respectively, at 1.5 V. This tendency matches well with that previously observed from the voltammetric experiments in 3-electrode configuration, confirming the validity of the methodology for assessing the performance of the aerogels for the electrochemical removal of ionic species. The incorporation of carbon black in the synthesis led to a significant increase in the electrosorption capacity of the electrodes. Capacitance values of 10.3, 7.1 and 6.5 mg/g were recorded for CAGW4/CB, CAGW6/CB and CAGW8/CB at 1.5 V, respectively. As seen in Table 5,

the desalting capacity of these materials is higher or similar to that reported for other carbon-based electrodes [45-49]. Otherwise, the pH value increased during the charge to values close to 9.5 and then decreased to 8 upon discharge. This effect is commonly attributed to the generation of OH$^-$ anions at the cathode because of the reduction of dissolved oxygen from the influent.

The kinetic response of the monolith to the adsorption of ions can be elucidated from the slope of the electrosorption curves at short times. These adsorption rate values were calculated per unit of area and volume and are shown in Fig. 8a and b for different applied cell voltages. They can be correlated to the kinetic of the ions transport from the electrolyte to the inner pores of the monolith where they are eventually adsorbed. Larger area and volumetric rates were measured for CAGW4 and CAGW4/CB regardless the applied voltage. These results confirm the good kinetic response of both samples, which is also in good agreement with the low R$_{pol}$ determined by impedance spectroscopy in powdered electrodes (Fig. 6). Small differences were observed between CAGW6 and CAGW8 samples and their composites with carbon black, when the area adsorption rate is measured. Interestingly, the volumetric adsorption rates reveal a beneficial effect of carbon black in CAGW6/CB and CAGW8/CB, regardless the applied voltage. Contrarily, this tendency is less evident for CAGW4/CB. Likely, the slight decrease in surface area and microporosity observed in CAGW4/CB, as compared to CAGW4, may hinder the beneficial effect of carbon black to the ionic migration, which is more clearly observed in those aerogels with a slow kinetic response.

4. Conclusions

We have synthesized mesoporous carbon aerogels with enhanced conductivity and electrochemical performance for the electro-assisted removal of sodium chloride

from saline water by a simple modification of the catalyzed polycondensation of resorcinol-formaldehyde mixtures. SEM images and the textural analysis of the samples showed that carbon black particles are nicely integrated within the aggregates of the activated aerogels, confirming the effectiveness of the method to produce highly homogeneous composites with high surface areas and porosity suitable for electrochemical applications. The addition of a small amount (ca. 0.9 wt.%) of carbon black during the sol-gel polymerization of the precursors did not modify the textural features of the aerogels, as opposed to the use of additive loadings above 5 wt.%, but significantly increased the electrochemical performance. Despite of this, the samples showed an enhanced electrochemical performance. The modified electrodes showed a much lower resistive response at low scan rates, although the amount of carbon black was too low to allow a fast charge propagation when high scan rates are used. The effect was more pronounced for aerogels prepared using low R/W molar ratio, which can be considered an interesting parameter to optimize the electrochemical performance of carbon aerogel electrodes.

Capacitance values of the unmodified control series followed the expected trend based on the textural parameters (surface area and micropore volume). In the case of the CAGWx/CB series, additional factors as the improved structural ordering, pore connectivity and the increase in the electrical conductivity provided by the crystalline carbon black phase account for the enhanced electrosorption capacity of these composites. The polarization resistance significantly increased with the R/W ratio, in close relation to the mesoporous network of the aerogels. Deionization experiments performed at several voltages evidenced the high electrosorption capacity for the carbon black-activated aerogel composite prepared with the lowest resorcinol-water ratio.

These experiments also revealed that ion migration through the whole monolith volume can be readily improved by the composite with homogeneously dispersed carbon black.

Acknowledgements

References

[1] J.E. Miller, Review of water resources and desalination technologies, SAND (2003) 2003-0800.

[2] M.A. Anderson, A.L. Cudero, J. Palma, Electrochim. Acta 55 (2010) 3845-3856.

[3] J. Yang, L. D. Zou, H. H. Song, Z. P. Hao, Desalination 276 (2011) 199–206.

[4] C. O. Ania, M. Haro, G. Rasines, C. Macias, Carbon 49 (2011) 3723-3730.

[5] T. J.Welgemoed, C. F. Schutte, Desalination 183 (2005) 327-340.

[6] M. Noked, A. Soffer, D. Aurbach, J. Solid State Electrochem. 15 (2011) 1563-1578.

[7] Z. Peng, D. S. Zhang, L. Y. Shi, T. T. Yan, S. Yuan, H. R. Li, R. H. Gao, J. H. Fang, J. Phys. Chem. C 115 (2011) 17068-17076.

[8] H. Wang, L.Y. Shi, T.T. Yan, J.P. Zhang, Q.D. Zhong, D.S. Zhang, J. Mater. Chem. A 2 (2014) 4739-4750.

[9] H. J. Yin, S. L. Zhao, J. W. Wan, H. J. Tang, L. Chang, L. C. He, H. J. Zhao, Y. Gao, Z. Y. Tang, Adv. Mater. 25 (2013) 6270-6276.

[10] I. Villar, S. Roldan, V. Ruiz, M. Granda, C. Blanco, R. Menéndez, R. Santamaría, Energy Fuels 24 (2010) 3329–3333.

[11] A. Ban, A. Schafer, H. Wendt, J Appl. Electrochem. 157 (1998) 602-615.

[12] D. Zhang, T. Yan, L. Shi, Z. Peng, X. Wen, J. Zhang, J Mater Chem 22 (2012) 14696-14704.

[13] P. Liang, L. Yuan, X. Yang, S. Zhou, X. Huang, Water. Res. 47 (2013) 2523-2530.

[14] G.P. Wu, J.B. Yang, D.P. Wang, R. Xu, K. Amine, C.X. Lu, Mater. Lett. 115 (2013) 1-4.

[15] L. Li, L. Zou, H. Song, G. Morris, Carbon 47 (2009) 775-781.

[16] X Wen, D Zhang, T Yan, H Wang, J Zhang, L Shi, J. Mater. Chem. A, 1 (2013) 12334-12344.

[17] T. Li , G. Yang, J. Wang, Y. Zhou, H. Han, J. Solid State Electrochem. 17 (2013) 2651-2660.

[18] H. Li, L. Zou, L. Pan, Z. Sun, Sep. Purif. Technol. 75 (2010) 8-14.

[19] H. Yin, S. Zhao, J. Wan, H. Tang, L. Chang, L. He, H. Zhao, Y. Gao, Z. Tang, Adv. Mater. 25 (2013), 6270-6276.

[20] J.J. Wouters, J.J. Lado, M.I. Tejedor-Tejedor, M.A. Anderson, J. Electrochem. Soc. 159 (2012) A1374.

[21] M.C. Zafra, P. Lavela, G. Rasines, C. Macías, J.L. Tirado, C.O. Ania, Electrochim. Acta 135 (2014) 208–216.

[22] M.T.Z. Myint, S.H. Al-Harthi, J. Dutta, Desalination 344 (2014) 236-242.

[23] R.W. Pekala, J.C. Farmer, C.T. Alviso, T.D. Tran, S.T. Mayer, J.M. Miller, B. Dunn, J. Non-Cryst Solids 225 (1998) 74-80.

[24] G. Rasines, P. Lavela, C. Macías, M. Haro, C.O. Ania, J. L. Tirado, J. Electroanal. Chem. 671 (2012) 92–98

[25] M. C. Zafra, P. Lavela, C. Macías, G. Rasines, J. L. Tirado, J. Electroanal. Chem. 708 (2013) 80–86

[26] C. Macías, P. Lavela, G. Rasines, M. C. Zafra, J. L. Tirado, C.O. Ania, J. Appl. Electrochem. 44 (2014) 963–976.

[27] H. Tamon, H. Ishizaka, M. Okazaki, Carbon 35 (1997) 791-796.

[28] Y. Yamamoto, T. Nishimura, T. Suzuki, H. Tamon, J. Non-Cryst. Solids 288(2001) 46-55.

[29] S.A. Al-Muhtaseb, J.A. Ritter, Adv. Mater. 15 (2003) 101-114.

[30] A.G. Pandolfo, A.F. Hollenkamp, J. Power Sources;157 (2006) 11-27.

[31] S. Nadakatti, M. Tendulkar, M. Kadam, Desalination 268 (2011) 182-188.

[32] K. Park, J. Lee, P. Park, S. Yoon, J. Moon, H. Eum, C. Lee, Desalination 206 (2007) 86-91.

[33] C. Macías, M. Haro, J. B. Parra, G. Rasines, C. O. Ania, Carbon 63 (2013) 487-497.

[34] F. Rouquerol, J. Rouquerol, K.S.W. Sing, P. Llewellyn, G. Maurin, Adsorption by Powders and Porous Solids, first ed., Elsevier, 2014.

[35] H. Tamon, H. Ishizaka, T. Araki, M. Okazaki, Carbon. 36 (1998) 1257-1262.

[36] D. Fairen-Jimenez, F. Carrasco-Marín, D. Jurado, F. Bley, F. Ehrburger-Dolle, C. Moreno-Castilla, J. Phys. Chem. B 10 (2006) 8681-8688.

[37] M. Seredych, D. Hulicova-Jurcakova, G. Q. Lu, T. J. Bandosz, Carbon 46 (2008) 1475-148.

[38] A. Stein, Z. Wang, M. A. Fierke, Adv. Mater. 21(2009) 265-293.

[39] A.P. Terzyk, Colloids Surf., A 177 (2001) 23-45.

[40] C.T. Hsieh, H. Teng, Carbon 40 (2002) 667-674.

[41] X. Wen, D. Zhang, L. Shi, T. Yan, H. Wang, J. Zhang, J. Mater. Chem. 22(2012) 23835-23844

[42] M. Noked, E. Avraham, A. Soffer, D. Aurbach, J. Phys. Chem. C 113 (2009) 21319-21327.

[43] J.M. Miller, B. Dunn Langmuir 15 (1999) 799–806.

[44] M. C. Zafra, P. Lavela, G. Rasines, C. Macías, J. L. Tirado, J. Solid State Electrochem. 18 (2014) 2847-2856.

[45] C.-H. Hou, C.-Y. Huang, Desalination 314 (2013) 124-129.

[46] H.-H. Jung, S.-W. Hwang, S.-H. Hyun, K.-H. Lee, G.-T. Kim, Desalination 216 (2007) 377-385.

[47] A.G. El-Deen, N.A. M. Barakat, K. A. Khalild, H.Y. Kim, New J. Chem. 38 (2014), 198-205.

[48] S. Wang, D. Wang, L. Ji, Q. Gong, Y.F. Zhu, J. Liang, Sep. Pur. Tech. 58 (2007) 12-16.

[49] C. Tsouris, R. Mayes, J. Kiggans, K. Sharma, S. Yiacoumi, D. DePaoli, S. Dai, Environ. Sci. Technol. 45 (2011) 10243-10249.

Table 1 Raman shift and width values for the D1 and G bands calculated from the deconvoluted spectra.

	R/W	I_G/I_{D1}	D1 shift (cm^{-1})	G shift (cm^{-1})	D1 FWHM (cm^{-1})	G FWHM (cm^{-1})
Control aerogels	0.04	0.78	1343.11	1594.37	155.19	76.27
	0.06	0.73	1344.26	1594.41	156.69	72.83
	0.08	0.71	1342.08	1594.69	146.53	67.30
Composites with carbon black	0.04	0.83	1342.72	1593.53	142.64	73.00
	0.06	0.78	1341.59	1593.50	149.83	72.98
	0.08	0.75	1342.88	1593.26	154.68	73.19

Table 2 BET surface area and pore volume values derived from the nitrogen isotherms measured for the aerogel samples.

Parameters	CAGW4	CAGW6	CAGW8	CAGW4/CB	CAGW6/CB	CAGW8/CB
S_{BET} / m^2 g^{-1}	954	862	894	903	854	856
$V_{MICRO}{}^{a}$ /cm^3 g^{-1}	0.22	0.20	0.21	0.21	0.20	0.20
V_{MESO} / cm^3 g^{-1}	2.21	1.25	0.92	2.13	1.29	0.94
$V_{TOTAL}{}^{b}$ / cm^3 g^{-1}	2.46	1.48	1.17	2.36	1.53	1.18

[a] Evaluated from DR equation.

[b] Evaluated at $p/p_o \sim 0.99$.

Table 3. XPS parameters calculated from the deconvolution of C1s, O1s spectra of activated carbon aerogels. (B.E.: Binding energy).

XPS data (envelope C1s)

B.E. /eV	Assigments	CAGW4	CAGW6	CAGW8	CAGW4/CB	CAGW6/CB	CAGW8/CB
284.6	C-C	66.1	67.1	69.3	60.1	64.3	66.8
286.1	C-OH	12.8	11.5	10.4	16.7	12.9	11.7
287.3	C=O	10.6	10.8	10.0	12.7	12.2	11.1
289.7	O-C=O	6.4	6.2	6.0	7.0	6.5	6.2
291.7	π-π*	4.2	4.4	4.3	3.5	4.1	4.2

XPS data (envelope O1s)

B.E /eV	Assigments	CAGW4	CAGW6	CAGW8	CAGW4/CB	CAGW6/CB	CAGW8/CB
530.9	carbonyl C=O	11.4	30.2	14.9	13.7	16.8	14.4
532.6	lactone, phenol, ether,C-OH	40.2	51.1	58.2	34.5	39.5	42.4
534.2	carboxyl COO-	39.8	15.3	17.6	46.7	36.7	32.8
536.1	Adsorbed H_2O or O_2; C=O in occluded CO_2, CO	8.6	3.4	9.3	5.2	7.1	10.4

Table 4. Atomic contents (%) of elements on the surfaces of the carbon aerogels determined by XPS.

	CAGW4	CAGW6	CAGW8	CAGW4/CB	CAGW6/CB	CAGW8/CB
C1s	95.27	95.19	95.43	93.45	94.44	94.40
O1s	4.73	4.81	4.57	6.45	5.56	5.60

Table 5. Comparison of the desalting capacity (mg NaCl/g electrode) of of various carbon electrodes.

Carbon material	Applied voltage (V)	Initial concentration (M)	Adsorption capacity (mg g^{-1})	Reference
Activated carbon	1.2	0.01	7.7	45
Carbon aerogel	1.5	0.017	7.0	46
CNF	1.2	1	1.91	47
CNT	1.2	0.5	9.35	48
RMCG	1.2	0.02	6.1	49

CNF: Carbon naonofiber; CNT:Carbon nanotube; RMCG: Resorcinol type mesocarbon coated graphite.

Figure captions

Fig. 1 TEM images of the activated aerogels and composites with carbon black. An image of pure carbon black (CB) has also been included for comparative purposes.

Fig. 2 X-ray diffraction patterns of the carbon black additive (CB), activated aerogels and their corresponding composites with carbon black. Diffractograms have been shifted for clarity.

Fig. 3 N_2 adsorption isotherms recorded at 77 K of the activated aerogels and composites with carbon black. Inset: Pore size distribution plots

Fig. 4 XPS spectra of a) CAGW4; c) CAGW6 and e) CAGW8 and composites with carbon black b) CAGW4/CB; d) CAGW6/CB and f) CAGW8/CB measured at the (A) C1s and (B) O1s core levels.

Fig. 5 Cyclic voltammograms of the activated aerogels a) CAGW4 and CAGW4/CB, b) CAGW6 and CAGW6/CB c) CAGW8 and CAGW8/CB. Open symbols (with carbon black), line (without carbon black).

Fig. 6 a) Nyquist plots from impedance spectra recorded for the activated aerogels and their corresponding composites with carbon black; b) Equivalent circuit applied to the fitting of the impedance spectra

Fig. 7 Electrosorption capacity of activated aerogels a) CAGW4; c) CAGW6 and e) CAGW8 and composites with carbon black b) CAGW4/CB; d) CAGW6/CB and f) CAGW8/CB. The symmetric batch cells with 0.025 M NaCl solution were subjected to constant voltage pulses of 0.9, 1.2 and 1.5 V.

Fig. 8 Adsorption rates of 0.1 M NaCl solution measured in symmetric batch cells for the activated aerogels and their corresponding composites with carbon black.

The electrodes were subjected at applied voltage pulses of 0.9, 1.2 and 1.5 V. the values are referred to the a) geometrical area of monoliths and b) volume of monoliths.
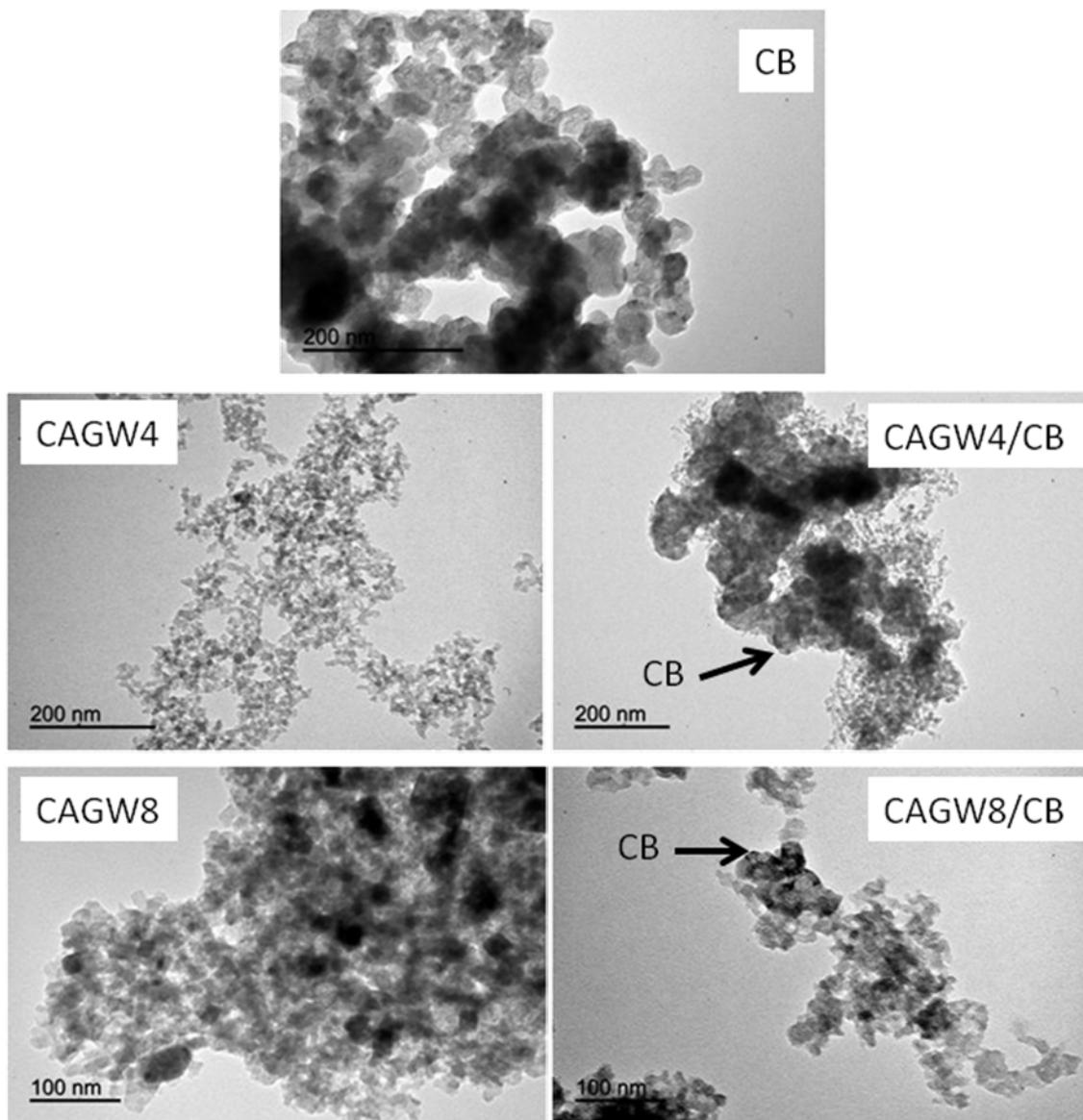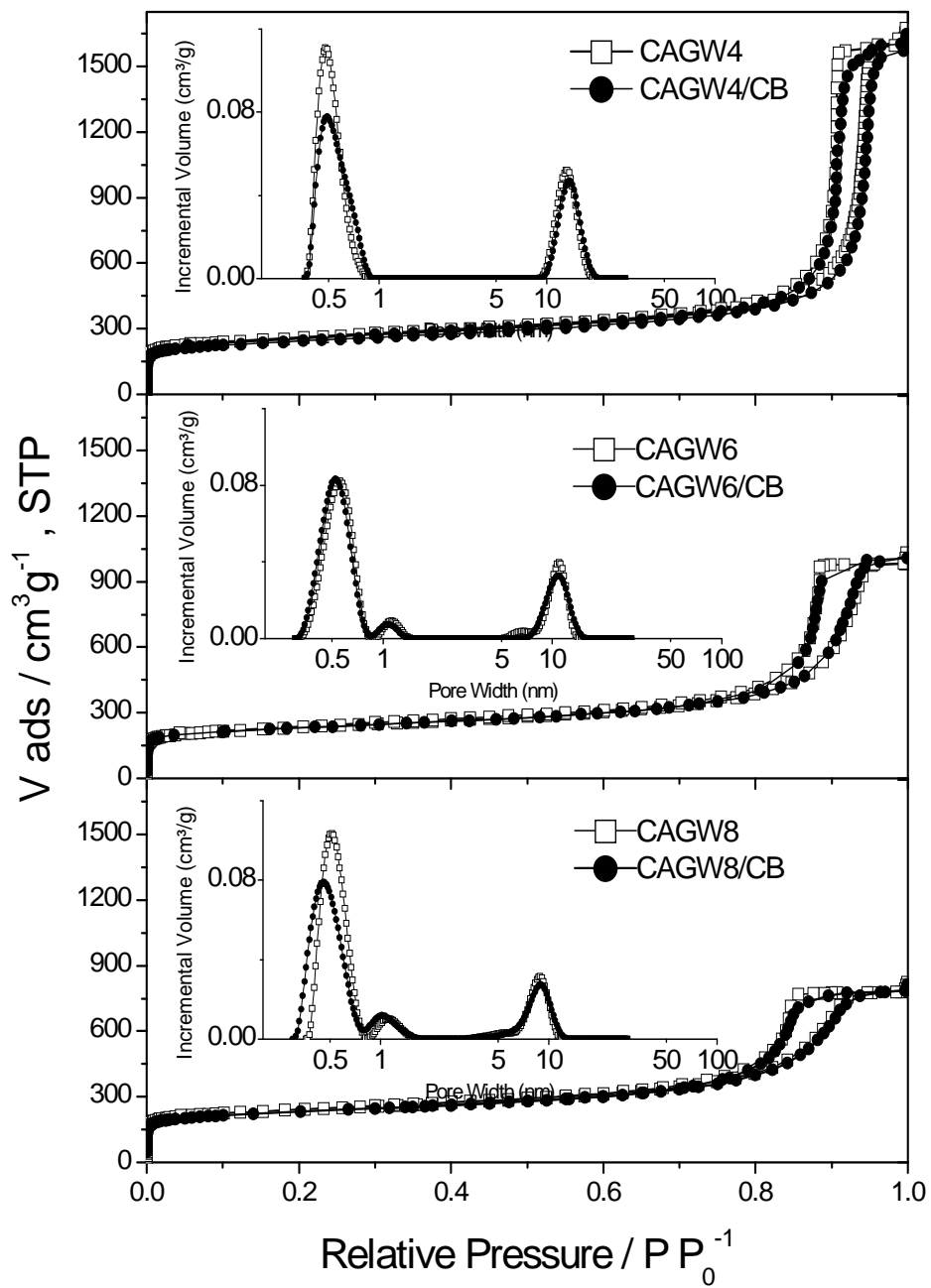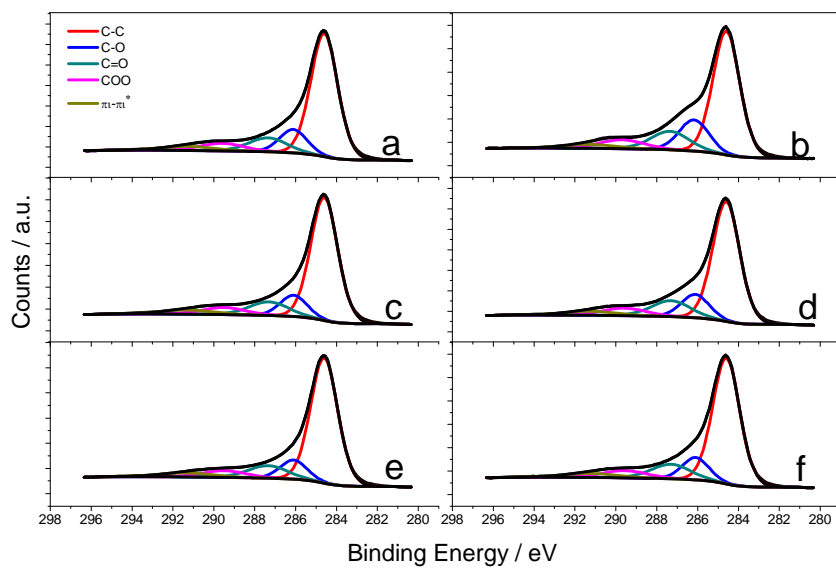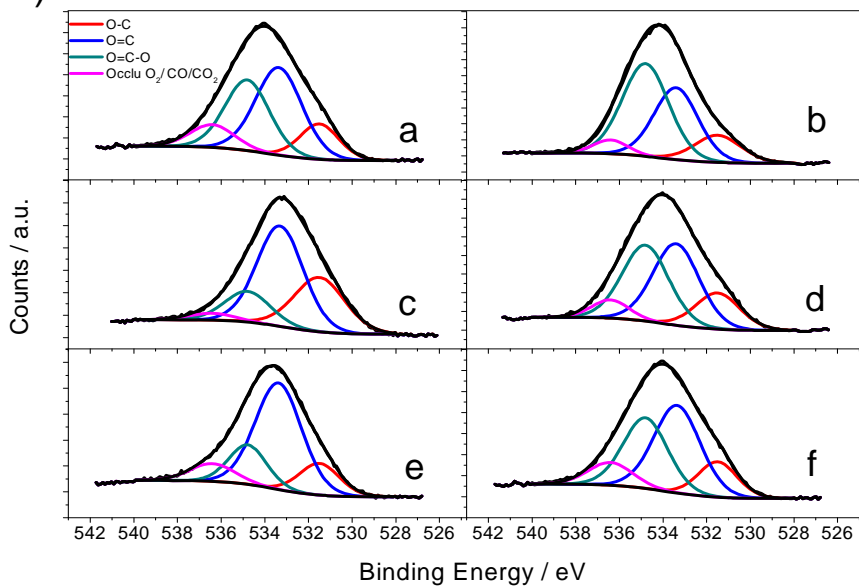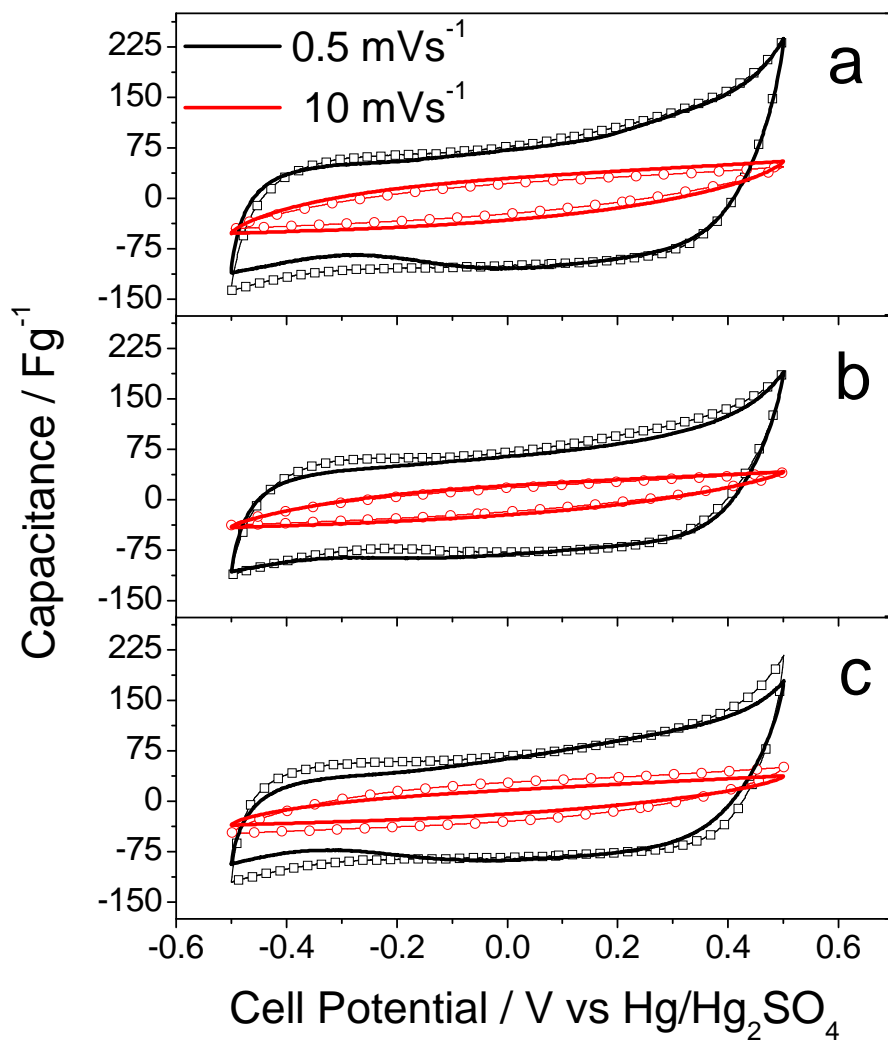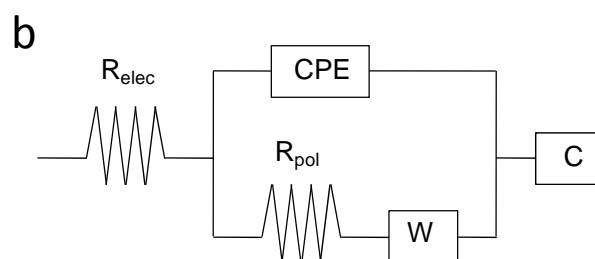
Figure 1
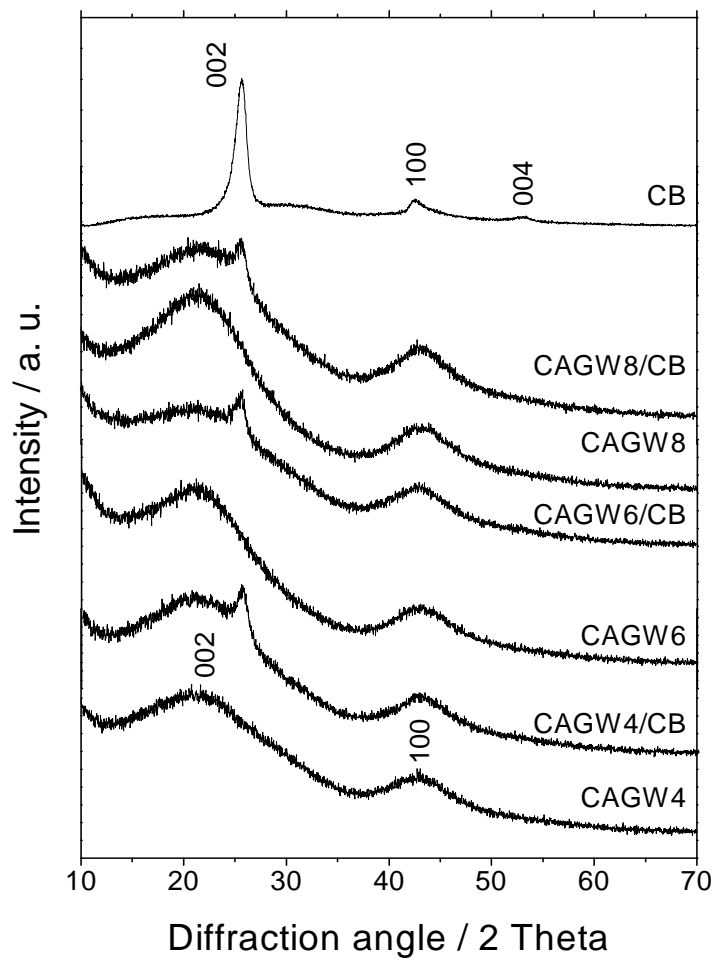
Figure 2

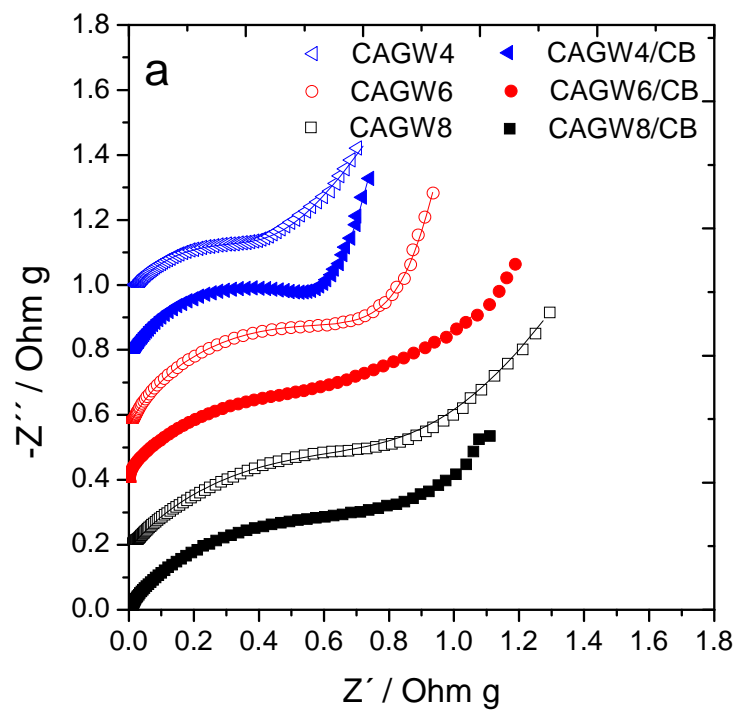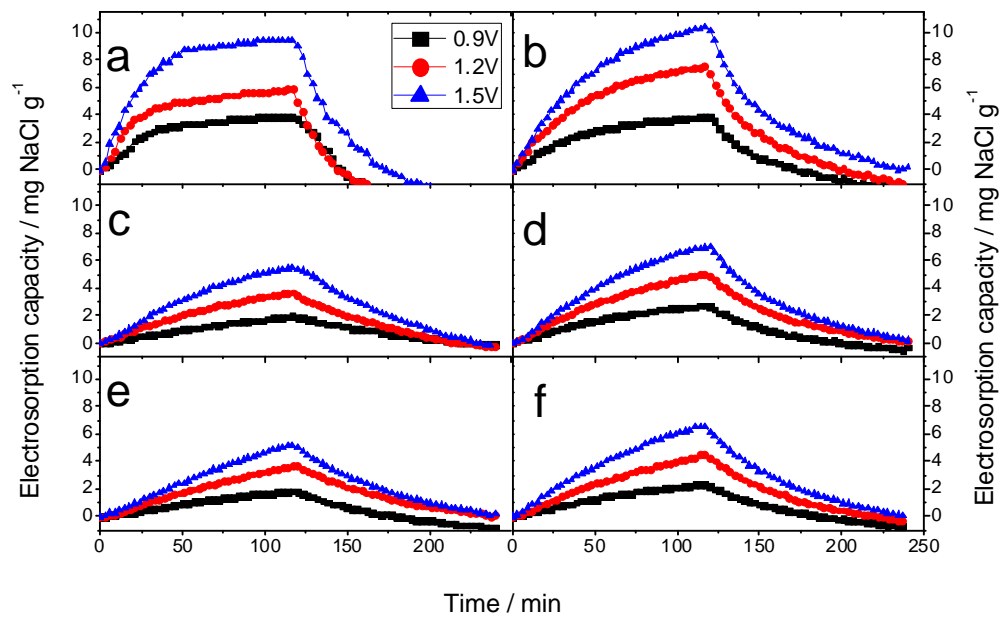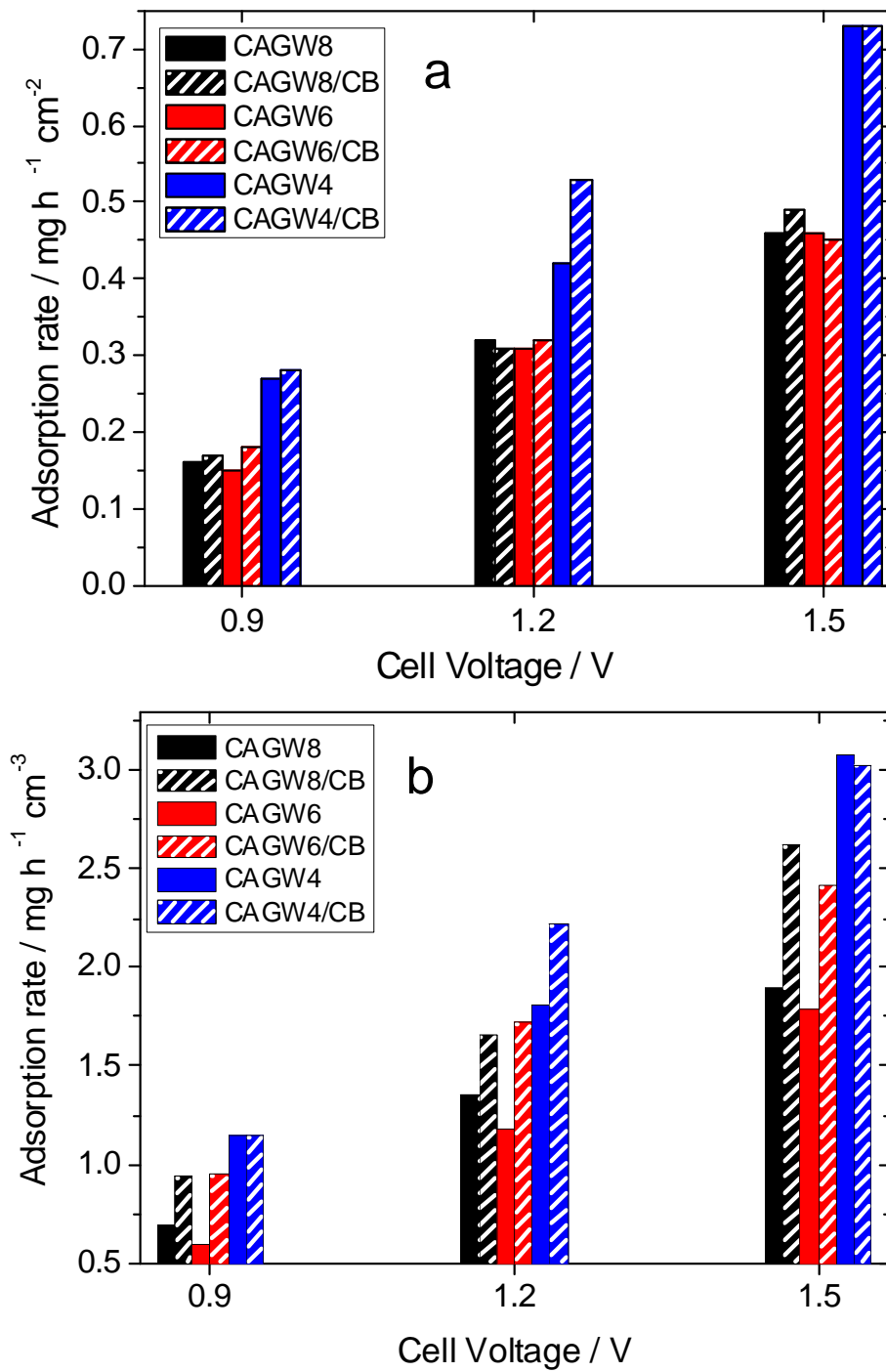Figure 3

Figure 4

Figure 5

Figure 6

Figure 7

Figure 8

Mesoporous carbon black-aerogel composites with optimized properties for the electro-assisted removal of sodium chloride from brackish water

SUPPLEMENTARY INFORMATION

G. Rasines[a], P. Lavela[b,*], C.O. Ania[c], C. Macías[a], M. C. Zafra[b], J. L. Tirado[b].

[a] Nanoquimia S.L., PCT Rabanales 21, Ed. Aldebarán M.4.7., 14014 Córdoba, Spain.
[b] Laboratorio de Química Inorgánica, Universidad de Córdoba, Marie Curie, Campus de Rabanales, 14071 Córdoba, Spain.
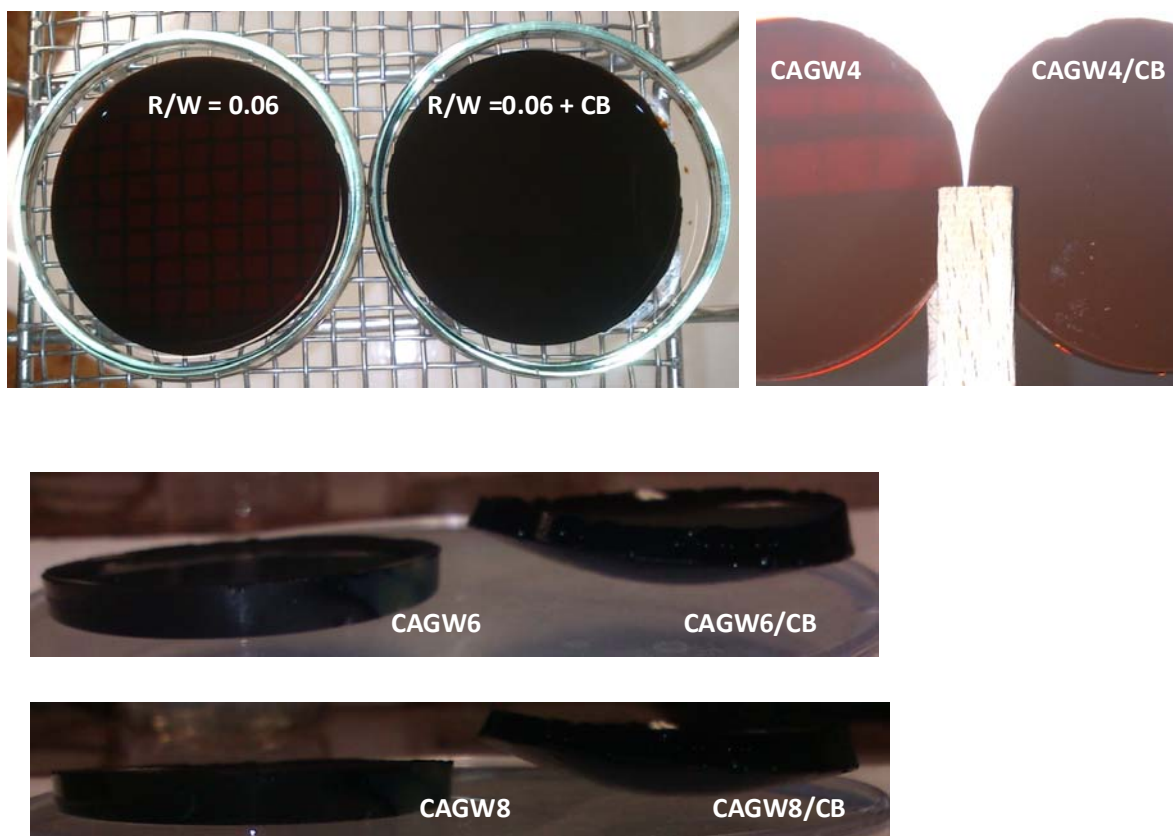[c] Instituto Nacional del Carbón (INCAR, CSIC), Apartado 73, 33080 Oviedo, Spain.

Fig. S1 Images of the synthesized aerogels, showing the differences in color and shape upon the incorporation of the carbon black additive to the difference R/W molar ratio.
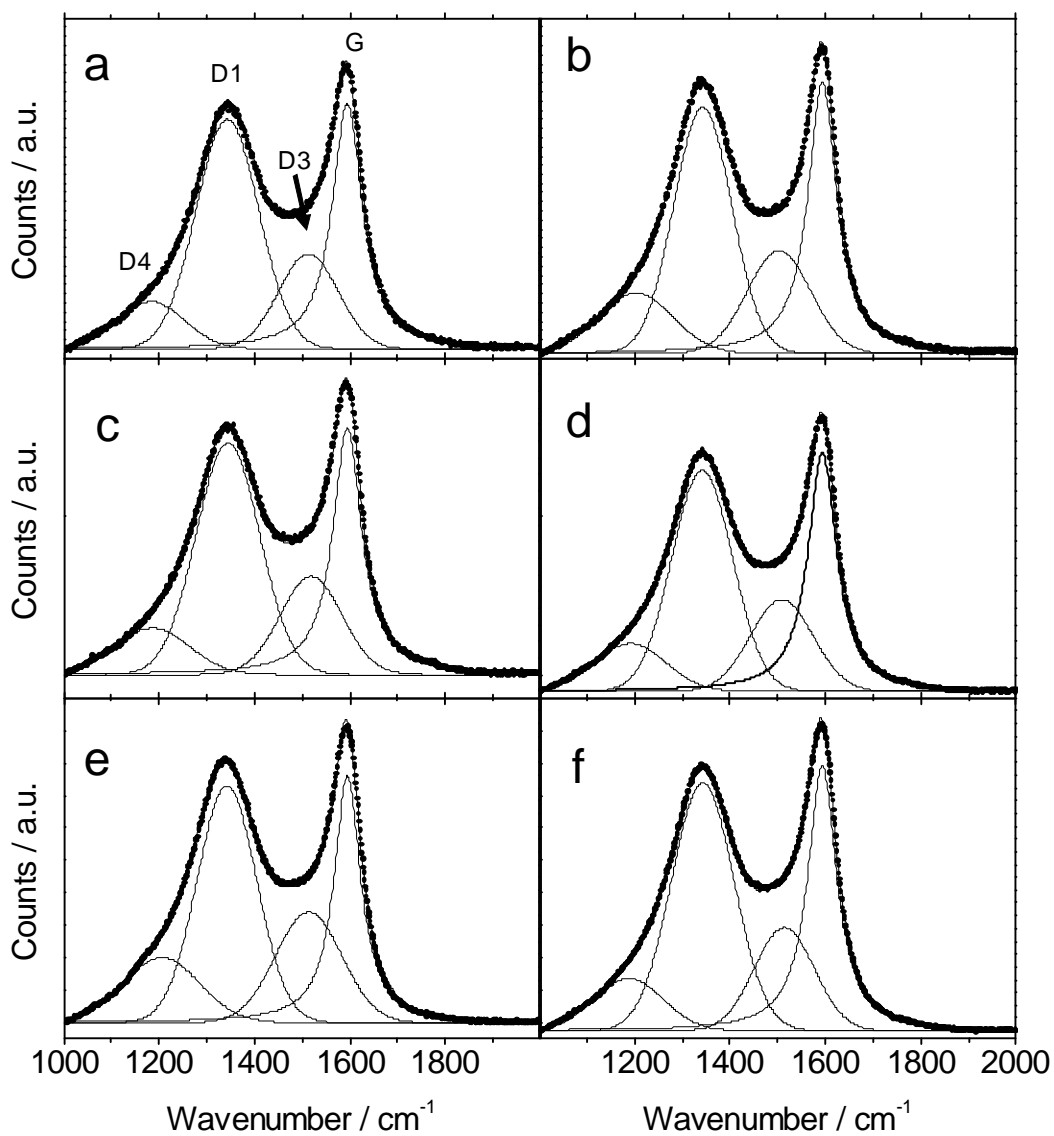
Fig. S2 Raman spectra of the activated aerogels a) CAGW4; c) CAGW6 and e) CAGW8 and composites with carbon black b) CAGW4/CB; d) CAGW6/CB and f) CAGW8/CB. The Raman modes are indicated in the figure.